Aerodynamic Design

by

A. Jameson

Department of Aeronautics and Astronautics
Stanford University, Stanford, California

Proceedings
Computational Science for the 21st Century

Tours
May 1997

Aerodynamic Design

Antony Jameson
Stanford University

1. INTRODUCTION

It is a pleasure to offer a contribution to the volume honoring the 60th birthday of Roland Glowinski. He has had a pervasive influence over the entire field of computational science and engineering. In the context of this paper it is particularly appropriate to re-call the work of the INRIA-Dassault group (including Pironneau, Periaux, Perrier, Poirier and Bristau) under his leadership, which developed new algorithms for the computation of transonic flow based on control theory. This enabled the finite element method to be adapted to problems of mixed type, allowing its exploitation to treat complex geometric configurations. By 1982 the group was able to carry out the first calculation of transonic potential flow around a complete aircraft [BPG+85]. This was a major advance that yielded immediate benefits at Dassault in their development of new aircraft.

Since 1988 much of the author's research has been focused on the development of methods for optimizing aerodynamic shapes for transonic and supersonic flow based on control theory [Jam88]. This work draws on many similar concepts to those used by the INRIA-Dassault group, though it differs in using a transformation to a fixed computational domain to simplify the formulation. Pironneau had earlier examined the problem of shape optimization for systems governed by elliptic equations [Pir84], and more recently has studied the optimization of flows governed by the incompressible Navier-Stokes equations. The present paper reviews the current status of the work of the author and his associates. Our method for aerodynamic shape design has recently been extended both to treat complex configurations and to optimize aerodynamic shapes for flows governed by the compressible Navier-Stokes equations. During the summer of 1996 it was used in a major industrial project: the design of the proposed McDonnell Douglas MDXX long range transport aircraft, and the paper touches on some of our experiences in this project.

Traditionally the process of selecting design variations has been carried out by trial and error, relying on the intuition and experience of the designer. It is not at all likely that repeated trials in an interactive design and analysis procedure can lead to a truly optimum design. In order to take full advantage of the possibility of examining a large design space the numerical simulations need to be combined with automatic search and optimization procedures. This can lead to automatic design methods which will fully realize the potential improvements in aerodynamic efficiency.

If the boundary shape is regarded as arbitrary within some requirements of smoothness, then the full generality of shapes cannot be defined with a finite number

of parameters, and one must use the concept of the Frechet derivative of the cost with respect to a function. Clearly, such a derivative cannot be determined directly by finite differences of the design parameters because there are now an infinite number of these. Using techniques of control theory, however, the gradient can be determined indirectly by solving an adjoint equation which has coefficients defined by the solution of the flow equations. The cost of solving the adjoint equation is comparable to that of solving the flow equations. Thus the gradient can be determined with roughly the computational cost of two flow solutions, independently of the number of design variables, which may be infinite if the boundary is regarded as a free surface.

Before embarking on a detailed derivation of the adjoint formulation for optimal Navier-Stokes equations, it is helpful to summarize the general abstract description of the adjoint approach which has been thoroughly documented in references [Jam88, JPM97]. The progress of the design procedure is measured in terms of a cost function I, which could be, for example the drag coefficient or the lift to drag ratio. For flow about an airfoil or wing, the aerodynamic properties which define the cost function are functions of the flow-field variables (w) and the physical location of the boundary, which may be represented by the function $\mathcal{F}$, say. Then

$$I = I(w, \mathcal{F}),$$

and a change in $\mathcal{F}$ results in a change

$$\delta I = \left[\frac{\partial I^T}{\partial w}\right]_I \delta w + \left[\frac{\partial I^T}{\partial \mathcal{F}}\right]_{II} \delta \mathcal{F} \tag{1}$$

in the cost function. Here, the subscripts I and II are used to distinguish the contributions due to the variation δw in the flow solution from the change associated directly with the modification $\delta \mathcal{F}$ in the shape. This notation is introduced to assist in grouping the numerous terms that arise during the derivation of the full Navier–Stokes adjoint operator, so that the basic structure of the approach as it is sketched in the present section can easily be recognized.

Suppose that the governing equation R which expresses the dependence of w and $\mathcal{F}$ within the flowfield domain D can be written as

$$R(w, \mathcal{F}) = 0. \tag{2}$$

Then δw is determined from the equation

$$\delta R = \left[\frac{\partial R}{\partial w}\right]_I \delta w + \left[\frac{\partial R}{\partial \mathcal{F}}\right]_{II} \delta \mathcal{F} = 0. \tag{3}$$

Next, introducing a Lagrange Multiplier ψ, we have

$$\begin{aligned}
\delta I &= \frac{\partial I^T}{\partial w}\delta w + \frac{\partial I^T}{\partial \mathcal{F}}\delta \mathcal{F} && (4)\\
&- \psi^T \left(\left[\frac{\partial R}{\partial w}\right] \delta w + \left[\frac{\partial R}{\partial \mathcal{F}}\right] \delta \mathcal{F} \right) && (5)\\
&= \left\{ \frac{\partial I^T}{\partial w} - \psi^T \left[\frac{\partial R}{\partial w}\right] \right\}_I \delta w && (6)\\
&+ \left\{ \frac{\partial I^T}{\partial \mathcal{F}} - \psi^T \left[\frac{\partial R}{\partial \mathcal{F}}\right] \right\}_{II} \delta \mathcal{F}. && (7)
\end{aligned}$$

Choosing ψ to satisfy the adjoint equation

$$\left[\frac{\partial R}{\partial w}\right]^T \psi = \frac{\partial I}{\partial w} \tag{8}$$

the first term is eliminated, and we find that

$$\delta I = \mathcal{G}\delta\mathcal{F}, \tag{9}$$

where

$$\mathcal{G} = \frac{\partial I^T}{\partial \mathcal{F}} - \psi^T \left[\frac{\partial R}{\partial \mathcal{F}}\right].$$

The advantage is that (9) is independent of δw, with the result that the gradient of I with respect to an arbitrary number of design variables can be determined without the need for additional flow-field evaluations. In the case that (2) is a partial differential equation, the adjoint equation (8) is also a partial differential equation and determination of the appropriate boundary conditions requires careful mathematical treatment.

Once equation (3) is established, an improvement can be made with a shape change

$$\delta\mathcal{F} = -\lambda\mathcal{G},$$

where λ is positive, and small enough that the first variation is an accurate estimate of δI. Then

$$\delta I = -\lambda\mathcal{G}^T\mathcal{G} < 0.$$

After making such a modification, the gradient can be recalculated and the process repeated to follow a path of steepest descent until a minimum is reached. In order to avoid violating constraints, such as a minimum acceptable wing thickness, the gradient may be projected into an allowable subspace within which the constraints are satisfied. In this way, procedures can be devised which must necessarily converge at least to a local minimum.

2. DESIGN USING THE NAVIER-STOKES EQUATIONS

It is convenient to use Cartesian coordinates (x_1,x_2,x_3) and to adopt the convention of indicial notation where a repeated index "i" implies summation over $i = 1$ to 3. The three-dimensional Navier-Stokes equations then take the form

$$\frac{\partial w}{\partial t} + \frac{\partial f_i}{\partial x_i} = \frac{\partial f_{vi}}{\partial x_i} \quad \text{in } \mathcal{D}, \tag{10}$$

where the state vector w, inviscid flux vector f and viscous flux vector f_v are described respectively by

$$w = \begin{Bmatrix} \rho \\ \rho u_1 \\ \rho u_2 \\ \rho u_3 \\ \rho E \end{Bmatrix}, \quad f_i = \begin{Bmatrix} \rho u_i \\ \rho u_i u_1 + p\delta_{i1} \\ \rho u_i u_2 + p\delta_{i2} \\ \rho u_i u_3 + p\delta_{i3} \\ \rho u_i H \end{Bmatrix}, \quad f_{vi} = \begin{Bmatrix} 0 \\ \sigma_{ij}\delta_{j1} \\ \sigma_{ij}\delta_{j2} \\ \sigma_{ij}\delta_{j3} \\ u_j\sigma_{ij} + k\frac{\partial T}{\partial x_i} \end{Bmatrix}. \tag{11}$$

In these definitions, ρ is the density, u_1, u_2, u_3 are the Cartesian velocity components, E is the total energy and δ_{ij} is the Kronecker delta function. The pressure is determined by the equation of state

$$p = (\gamma - 1)\,\rho \left\{ E - \frac{1}{2}\,(u_i u_i) \right\},$$

and the stagnation enthalpy is given by

$$H = E + \frac{p}{\rho},$$

where γ is the ratio of the specific heats. The viscous stresses may be written as

$$\sigma_{ij} = \mu \left(\frac{\partial u_i}{\partial x_j} + \frac{\partial u_j}{\partial x_i} \right) + \lambda \delta_{ij} \frac{\partial u_k}{\partial x_k},$$

where μ and λ are the first and second coefficients of viscosity. The coefficient of thermal conductivity and the temperature are defined by

$$k = \frac{\gamma \mu}{Pr}, \qquad T = \frac{p}{(\gamma - 1)\rho}. \tag{12}$$

For discussion of real applications using a discretization on a body conforming structured mesh, it is useful to consider a transformation to the computational coordinates (ξ_1,ξ_2,ξ_3) defined by the metrics

$$K_{ij} = \left[\frac{\partial x_i}{\partial \xi_j} \right], \quad J = \det(K), \quad K_{ij}^{-1} = \left[\frac{\partial \xi_i}{\partial x_j} \right].$$

The Navier-Stokes equations can then be written in computational space as

$$\frac{\partial (Jw)}{\partial t} + \frac{\partial (F_i - F_{vi})}{\partial \xi_i} = 0 \quad \text{in } \mathcal{D}, \tag{13}$$

where the inviscid and viscous flux contributions are now defined with respect to the computational cell faces by $F_i = S_{ij} f_j$ and $F_{vi} = S_{ij} f_{vj}$, and the quantity $S_{ij} = J K_{ij}^{-1}$ is used to represent the projection of the ξ_i cell face along the x_j axis. For convenience, the coordinates ξ_i describing the fixed computational domain are chosen so that each boundary conforms to a constant value of one of these coordinates. Variations in the shape then result in corresponding variations in the mapping derivatives defined by K_{ij}.

Suppose that the performance is measured by a cost function

$$I = \int_{\mathcal{B}} \mathcal{M}(w, S)\, dB_\xi + \int_{\mathcal{D}} \mathcal{P}(w, S)\, dD_\xi,$$

containing both boundary and field contributions where dB_ξ and dD_ξ are the surface and volume elements in the computational domain. In general, $\mathcal{M}$ and $\mathcal{P}$ will depend on both the flow variables w and the metrics S defining the computational space. The design problem is now treated as a control problem where the boundary shape

represents the control function, which is chosen to minimize I subject to the constraints defined by the flow equations (13). A shape change produces a variation in the flow solution δw and the metrics δS which in turn produce a variation in the cost function

$$\delta I = \int_{\mathcal{B}} \delta\mathcal{M}(w,S)\, d\mathcal{B}_\xi + \int_{\mathcal{D}} \delta\mathcal{P}(w,S)\, d\mathcal{D}_\xi, \tag{14}$$

with

$$\begin{aligned} \delta\mathcal{M} &= [\mathcal{M}_w]_I\, \delta w + \delta\mathcal{M}_{II}, \\ \delta\mathcal{P} &= [\mathcal{P}_w]_I\, \delta w + \delta\mathcal{P}_{II}, \end{aligned} \tag{15}$$

where we continue to use the subscripts I and II to distinguish between the contributions associated with the variation of the flow solution δw and those associated with the metric variations δS. Thus $[\mathcal{M}_w]_I$ and $[\mathcal{P}_w]_I$ represent $\frac{\partial\mathcal{M}}{\partial w}$ and $\frac{\partial\mathcal{P}}{\partial w}$ with the metrics fixed, while $\delta\mathcal{M}_{II}$ and $\delta\mathcal{P}_{II}$ represent the contribution of the metric variations δS to $\delta\mathcal{M}$ and $\delta\mathcal{P}$.

In the steady state, the constraint equation (13) specifies the variation of the state vector δw by

$$\frac{\partial}{\partial\xi_i}\delta\left(F_i - F_{vi}\right) = 0. \tag{16}$$

Here δF_i and δF_{vi} can also be split into contributions associated with δw and δS using the notation

$$\begin{aligned} \delta F_i &= [F_{iw}]_I\, \delta w + \delta F_{iII} \\ \delta F_{vi} &= [F_{viw}]_I\, \delta w + \delta F_{viII}. \end{aligned} \tag{17}$$

The inviscid contributions are easily evaluated as

$$[F_{iw}]_I = S_{ij}\frac{\partial f_i}{\partial w}, \quad \delta F_{viII} = \delta S_{ij} f_j.$$

The details of the viscous contributions are complicated by the additional level of derivatives in the stress and heat flux terms.

Multiplying by a co-state vector ψ, which will play an analogous role to the Lagrange multiplier introduced in equation (7), and integrating over the domain produces

$$\int_{\mathcal{D}} \psi^T \frac{\partial}{\partial\xi_i}\delta\left(F_i - F_{vi}\right) = 0. \tag{18}$$

If ψ is differentiable this may be integrated by parts to give

$$\int_{\mathcal{B}} n_i \psi^T \delta\left(F_i - F_{vi}\right) d\mathcal{B}_\xi \tag{19}$$

$$- \int_{\mathcal{D}} \frac{\partial\psi^T}{\partial\xi_i}\delta\left(F_i - F_{vi}\right) d\mathcal{D}_\xi = 0. \tag{20}$$

Since the left hand expression equals zero, it may be subtracted from the variation in the cost function (14) to give

$$\begin{aligned} \delta I &= \int_{\mathcal{B}} \left[\delta\mathcal{M} - n_i\psi^T\delta\left(F_i - F_{vi}\right)\right] d\mathcal{B}_\xi \\ &+ \int_{\mathcal{D}} \left[\delta\mathcal{P} + \frac{\partial\psi^T}{\partial\xi_i}\delta\left(F_i - F_{vi}\right)\right] d\mathcal{D}_\xi. \end{aligned} \tag{21}$$

Now, since ψ is an arbitrary differentiable function, it may be chosen in such a way that δI no longer depends explicitly on the variation of the state vector δw. The gradient of the cost function can then be evaluated directly from the metric variations without having to recompute the variation δw resulting from the perturbation of each design variable.

Comparing equations (15) and (17), the variation δw may be eliminated from (21) by equating all field terms with subscript "I" to produce a differential adjoint system governing ψ

$$\frac{\partial \psi^T}{\partial \xi_i} \left[F_{j_w} - F_{v j_w} \right]_I + \mathcal{P}_w = 0 \quad \text{in } \mathcal{D}. \tag{22}$$

The corresponding adjoint boundary condition is produced by equating the subscript "I" boundary terms in equation (21) to produce

$$n_i \psi^T \left[F_{j_w} - F_{v j_w} \right]_I = \mathcal{M}_w \quad \text{on } \mathcal{B}. \tag{23}$$

The remaining terms from equation (21) then yield a simplified expression for the variation of the cost function which defines the gradient

$$\begin{aligned} \delta I &= \int_{\mathcal{B}} \left\{ \delta \mathcal{M}_{II} - n_i \psi^T \left(F_i - F_{vi} \right) \right\} d\mathcal{B}_\xi \\ &+ \int_{\mathcal{D}} \left\{ \delta \mathcal{P}_{II} + \left[\delta F_i - \delta F_{vi} \right]_{II} \right\} d\mathcal{D}_\xi, \end{aligned} \tag{24}$$

Taking the transpose of equation (22), the inviscid adjoint equation may be written as

$$C_i^T \frac{\partial \psi}{\partial \xi_i} = 0 \quad \text{in } \mathcal{D}, \tag{25}$$

where the inviscid Jacobian matrices in the transformed space are given by

$$C_i = S_{ij} \frac{\partial f_j}{\partial w}.$$

The derivation of the viscous adjoint terms is simplified by transforming to the primitive variables

$$\tilde{w}^T = (\rho, u_1, u_2, u_3, p)^T,$$

because the viscous stresses depend on the velocity derivatives $\frac{\partial u_i}{\partial x_j}$, while the heat fluxes can be expressed as

$$k \frac{\partial}{\partial x_i} \left(\frac{p}{\rho} \right).$$

The relationship between the conservative and primitive variations are defined by the expressions

$$\delta w = M \delta \tilde{w}, \quad \delta \tilde{w} = M^{-1} \delta w,$$

which make use of the transformation matrices $M = \frac{\partial w}{\partial \tilde{w}}$ and $M^{-1} = \frac{\partial \tilde{w}}{\partial w}$. The conservative and primitive adjoint operators L and $\tilde{L}$ corresponding to the variations δw and $\delta \tilde{w}$ are then related by

$$\int_{\mathcal{D}} \delta w^T L \psi \, d\mathcal{D}_\xi = \int_{\mathcal{D}} \delta \tilde{w}^T \tilde{L} \psi \, d\mathcal{D}_\xi,$$

with

$$\tilde{L} = M^T L,$$

where

$$M^T = \begin{bmatrix} 1 & u_1 & u_2 & u_3 & \frac{u_i u_i}{2} \\ 0 & \rho & 0 & 0 & \rho u_1 \\ 0 & 0 & \rho & 0 & \rho u_2 \\ 0 & 0 & 0 & \rho & \rho u_3 \\ 0 & 0 & 0 & 0 & \frac{1}{\gamma - 1} \end{bmatrix}$$

The details of the derivation of the viscous adjoint operator are provided in [JPM97] with the simplification that variations in the transport coefficients are ignored. Collecting together the contributions from the momentum and energy equations, the viscous adjoint operator in primitive variables can finally be expressed as

$$\begin{aligned} (\tilde{L}\psi)_1 &= -\frac{p}{(\gamma-1)\rho^2}\frac{\partial}{\partial \xi_l}\left(S_{lj} k \frac{\partial \theta}{\partial x_j}\right) \\ (\tilde{L}\phi)_i &= \frac{\partial}{\partial \xi_l}\left\{S_{lj}\left[\mu\left(\frac{\partial \phi_i}{\partial x_j} + \frac{\partial \phi_j}{\partial x_i}\right) + \lambda \delta_{ij}\frac{\partial \phi_k}{\partial x_k}\right]\right\} \\ &+ \frac{\partial}{\partial \xi_l}\left\{S_{lj}\left[\mu\left(u_i\frac{\partial \theta}{\partial x_j} + u_j\frac{\partial \theta}{\partial x_i}\right) + \lambda \delta_{ij}\frac{\partial \theta}{\partial x_k}\right]\right\} \\ &- \sigma_{ij} S_{lj}\frac{\partial \theta}{\partial x_l} \\ (\tilde{L}\theta) &= \frac{\rho}{(\gamma-1)}\frac{\partial}{\partial \xi_l}\left(S_{lj} k \frac{\partial \theta}{\partial x_j}\right). \end{aligned}$$

The conservative viscous adjoint operator may then be obtained by the transformation

$$L = {M^{-1}}^T \tilde{L}.$$

The details of the formula for the gradient depend on the way in which the boundary shape is parameterized as a function of the design variables, and the way in which the mesh is deformed as the boundary is modified. Using the relationship between the mesh deformation and the surface modification, the field integral is reduced to a surface integral by integrating along the coordinate lines emanating from the surface. Thus the expression (26) for δI is finally reduced to the form of equation (9)

$$\delta I = \int_{\mathcal{B}} \mathcal{G}\delta\mathcal{F}\, d\mathcal{B}_\xi$$

where $\mathcal{F}$ represents the design variables, and $\mathcal{G}$ is the gradient, which is a function defined over the boundary surface.

The boundary conditions satisfied by the flow equations restrict the form of the left hand side of the adjoint boundary condition (23). Consequently, the boundary contribution to the cost function $\mathcal{M}$ cannot be specified arbitrarily. Instead, it must be chosen from the class of functions which allow cancellation of all terms containing δw in the boundary integral of equation (21). On the other hand, there is no such restriction on the specification of the field contribution to the cost function $\mathcal{P}$, since these terms may always be absorbed into the adjoint field equation (22) as source terms.

3. INDUSTRIAL APPLICATION

Due to the high computational cost of viscous design, a two-stage design strategy has been adopted. In the first stage, a design calculation is performed with the Euler equations to minimize the drag at a given lift coefficient by modifying the wing sections with a fixed planform. In the second stage, the pressure distribution of the Euler solution is used as the target pressure distribution for inverse design with the Navier-Stokes equations. Comparatively small modifications are required in the second stage, so that it can be accomplished with a small number of design cycles.

For verification purposes, this strategy was used for the re-design of a wing representative of wide body transport aircraft. The results are shown in Figures 1 and 2. The design point was taken as a lift coefficient of .55 at a Mach number of .83. Figure 1 illustrates the Euler redesign, which was performed on a mesh with $192\times32\times48$ cells, displaying both the geometry and the upper surface pressure distribution, with negative Cp upwards. The initial wing shows a moderately strong shock wave across most of the top surface, as can be seen in Figure 1a. Sixty design cycles were needed to produce the shock free wing shown in Figure 1b, with an indicated drag reduction of 15 counts from .0196 to .0181. Figure 2 shows the viscous redesign at a Reynolds number of 12 million. This was performed on a mesh with $192\times64\times48$ cells, with 32 intervals normal to the wing concentrated inside the boundary layer region. In Figure 2a it can be seen that the Euler design produces a weak shock due to the displacement effects of the boundary layer. Ten design cycles were needed to recover the shock free wing shown in Figure 2b. It is interesting that the wing section modifications between the initial wing of Figure 1a and the final wing of Figure 2b are remarkably small.

These results were sufficiently promising that it was decided by McDonnell Douglas to evaluate the method for industrial use, and it was used to support design studies for the MDXX project. Reference [Jam97] provides a more detailed discussion of the results of this experience. Early in the project it became apparent that the fuselage effects are too large to be ignored and that optimization at a single design point could lead to unsatisfactory off-design performance. Therefore we focused on the optimization of wing-body combinations at three design points. In viscous design it was also found that there were discrepancies between the results of the design calculations, which were initially performed on a relatively coarse grid with $192\times64\times48$ cells, and the results of subsequent analysis calculations performed on finer meshes to verify the design.

In order to allow the use of finer meshes with overnight turnaround, the code was therefore modified for parallel computation. Using the parallel implementation, viscous design calculations have been performed on meshes with 1.8 million mesh points. Starting from a preliminary inviscid design, 20 design cycles are usually sufficient for a viscous re-design in inverse mode, with the smoothed inviscid results providing the target pressure. Such a calculation can be completed in about $7\frac{1}{2}$ hours using 48 processors of an IBM SP2.

As an illustration of the results that could be obtained, Figure 3 shows a wing-body design with sweep back of about 38 degrees at the 1/4 chord. Starting from the result of an Euler design, the viscous optimization produced an essentially shock free wing at a cruise design point of Mach .86, with a lift coefficient of .6 for the wing body combination at a Reynolds number of 101 million based on the root chord. Figure

3 shows the design point, while the evolution of the design is shown in Figure 4, using software provided by J. Vassberg of Douglas Aircraft. In this case the pressure contours are for the final design. This wing is quite thick, with a thickness to chord ratio of more than 14 percent at the root and 9 percent at the tip. The design offers excellent performance at the nominal cruise point. Figures 5 and 6 show the results of a Mach number sweep to determine the drag rise. It can be seen that a double shock pattern forms below the design point, while there is actually a slight increase in the drag coefficient of about 1 $\frac{1}{2}$ counts at Mach .85. The tendency to produce double shocks below the design point is typical of supercritical wings. This wing has a low drag coefficient, however, over a wide range of conditions.

The final phase of the study, which was truncated by the cancellation of the MDXX, addressed the performance of the wing-body combination with engines and winglets included. Using GRIDGEN several weeks were needed to generate a mesh with 234 blocks and more than 5 million mesh cells. RANS calculations could then be performed in 5 or 6 hours with 48 processors of an IBM SP2. An example of such a calculation is presented in Figure 7, in which the shading indicates the surface pressure, with darker shading corresponding to higher pressure. The overall turn-around for mesh generation and flow analysis is still too slow for really effective use in a design project. Also one should in the future use optimization in the design of the complete configuration. A multiblock optimization code to treat complex configurations in which the flow is modeled by the Euler equations is already operational [Jam97]. A multiblock viscous design code is clearly needed and we plan to undertake its development. In the long run unstructured meshes may be needed to treat complete configurations with rapid turn-around.

Two major lessons of the studies were:

1. Useful simulations in the design of a wing for a commercial transport must treat at least wing-fuselage combinations and include viscous effects: more complete simulations ought to treat the engines, and also winglets if they are featured in the design.
2. To be fully accepted by the design team both CFD and optimization methods need to be validated before their use in the project.

It is clear, however, that optimization techniques of this type can both substantially reduce the cost of aerodynamic design, and improve the final results. In this case it enabled a team of four people (J. Alonso, J. Reuther, L. Martinelli and the author) to design a highly competitive wing in three months, starting from scratch.

ACKNOWLEDGMENT

This work has benefited from the generous support of AFOSR under Grant No. AFOSR-91-0391, DOD/URI/ONR/ARPA under Grant No. N00014-92-J-1796 and the NASA-IBM Cooperative Research Agreement.

REFERENCES

[BPG+85] Bristeau M., Pironneau O., Glowinski R., Periaux J., Perrier P., and Poirier G. (1985) On the numerical solution of nonlinear problems in fluid dynamics by least squares and finite element methods (II). application to transonic flow simulations. In Doltsinis J. S. (ed) *Proceedings of the 3rd International Conference on Finite Element Methods in Nonlinear Mechanics, FENOMECH 84, Stuttgart, 1984*, pages 363–394. North Holland.

[Jam88] Jameson A. (1988) Aerodynamic design via control theory. *J. Sci. Comp.* 3: 233–260.

[Jam97] Jameson A. (January 1997) Reengineering the design process through computation. *AIAA paper 97-0641.*

[JPM97] Jameson A., Pierce N., and Martinelli L. (January 1997) Optimum aerodynamic design using the Navier-Stokes equations. *AIAA paper 97-0101.*

[Pir84] Pironneau O. (1984) *Optimal Shape Design for Elliptic Systems.* Springer-Verlag, New York.

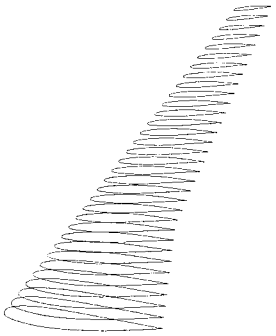

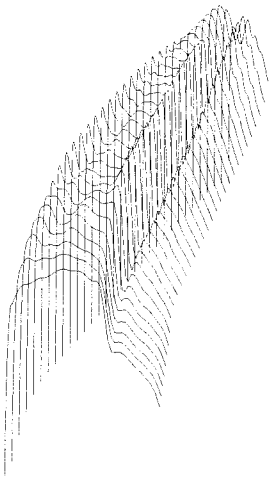

Initial Wing. C_p on Upper Surface.

Figure 1a: $M = .83, C_l = .5498, C_d = .0196, \alpha = 2.410°$.

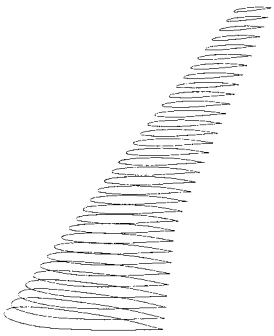

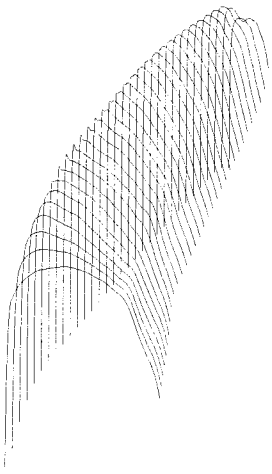

Redisigned wing. C_p on Upper Surface.

Figure 1b: $M = .83, C_l = .5500, C_d = .0181, \alpha = 1.959°$.

Figure 1 Redesign of the wing of a wide transport aircraft. Stage 1 Inviscid design : 60 design cycles in drag reduction mode with forced lift.

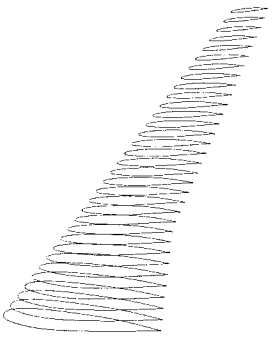

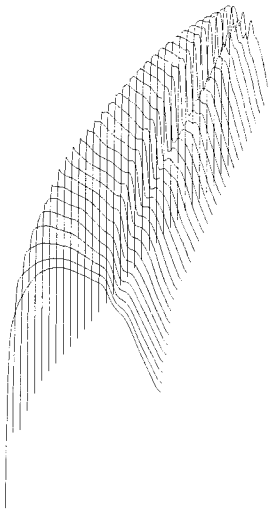

Initial Wing. C_p on Upper Surface.

Figure 2a: $M = 0.83, C_l = .5506, C_d = .0199, \alpha = 2.317°$

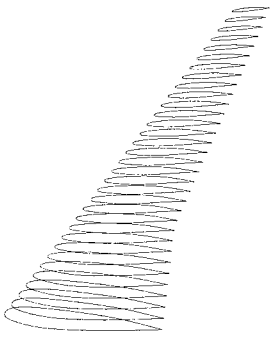

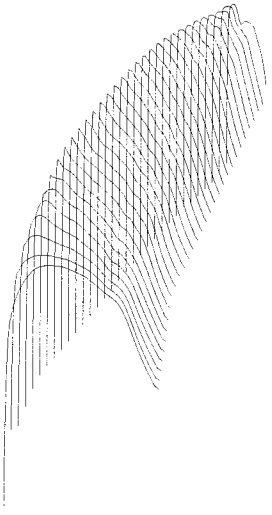

Redisigned wing. C_p on Upper Surface.

Figure 2b: $M = 0.83, C_l = .5508, C_d = .0194, \alpha = 2.355°$

Figure 2 Redesign of the wing of a wide transport aircraft. Stage 2: Viscous re-design. 10 design cycles in inverse mode.

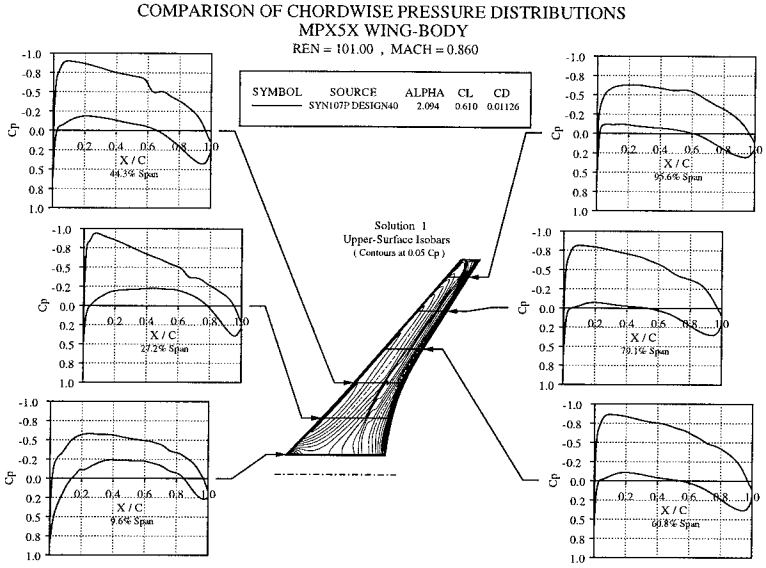

Figure 3 Pressure distribution of the MPX5X at its design point.

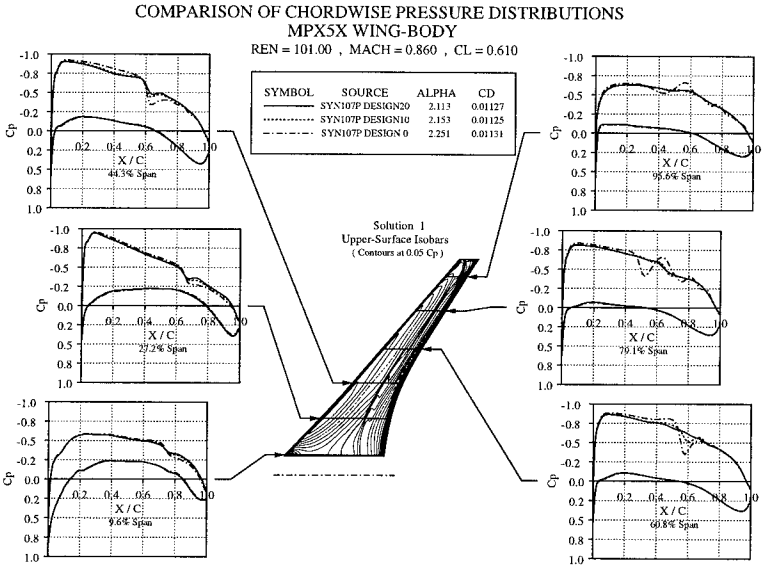

Figure 4 Optimization Sequence in the design of the MPX5X.

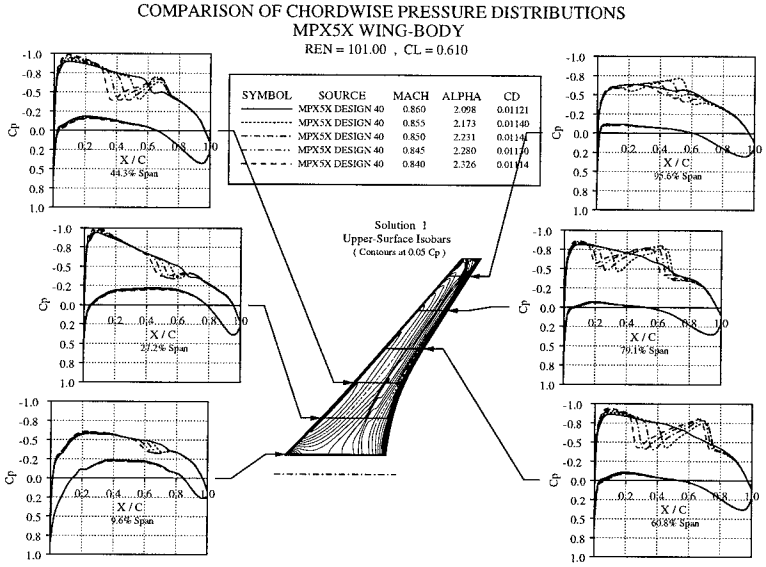

Figure 5 Off design performance of the MPX5X below the design point.

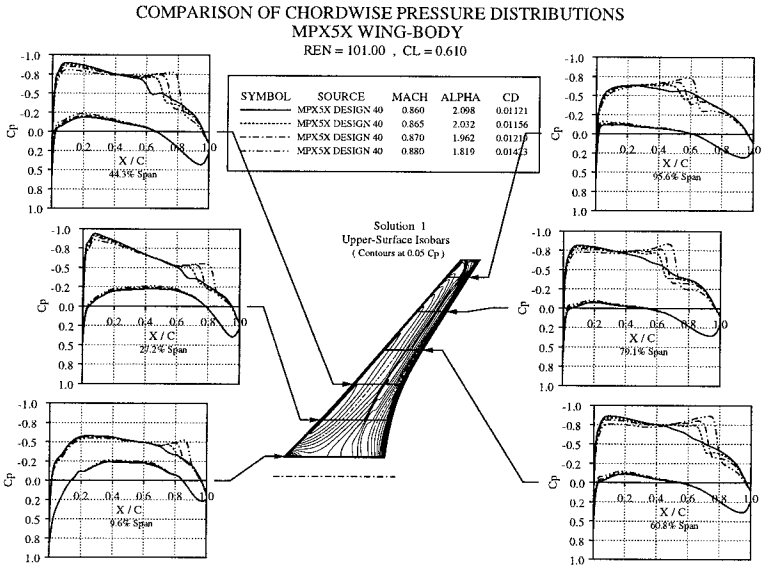

Figure 6 Off design performance of the MPX5X above the design point.

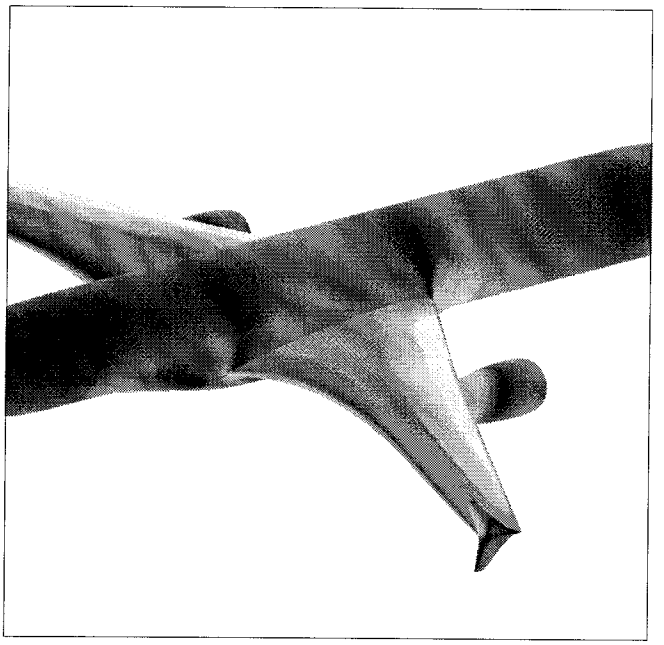

Figure 7 MPX3R wing-body-nacelle- winglet combination at Mach .85, CL = .6 . View from above.